Improved high resolution ocean reanalyses using a simple smoother algorithm

Article

Published Version

It is advisable to refer to the publisher's version if you intend to cite from the work. See Guidance on citing.

To link to this article DOI: http://dx.doi.org/10.1029/2021MS002626

www.reading.ac.uk/centaur

CentAUR

Central Archive at the University of Reading

Reading's research outputs online

Improved High Resolution Ocean Reanalyses Using a Simple Smoother Algorithm

Bo Dong[1] , **Keith Haines[1]** , and **Matthew Martin[2]**

[1]National Centre for Earth Observation, Department of Meteorology, University of Reading, Reading, UK, [2]Met Office, Exeter, UK

Abstract We present a simple smoother designed for smooth data adjustments in sequentially generated reanalysis products by utilizing knowledge of future assimilation increments. A decay time parameter is applied to the smoother increments to account for memory decay timescales in the ocean. The result is different from simply time smoothing the reanalysis itself as only the increments are smoothed so the reanalysis product can retain high frequency variability that is being internally generated by the model and the atmospheric forcing. The smoother is applied first to the Lorenz 1963 model and then to the daily Met Office GloSea5 Global ¼° ocean reanalysis during 2016. Results show significant improvement over the original reanalysis in the 3D temperature and salinity state and variability, as well as in the sea surface height (SSH) and ocean currents. Comparisons are made directly against temperature, salinity and SSH observations, as well as independent 15 m drifter velocities. The impact on the time variability of conservative quantities, particularly ocean heat and salt content, as well as kinetic energy and the Atlantic Meridional Overturning Circulation (AMOC), is also demonstrated.

Plain Language Summary The ocean observing system is sparse and ocean circulation is slow relative to the atmosphere, giving the system a longer memory of state properties. Therefore an ocean reanalysis could seek to use more "future data" to help produce the best historical ocean state reconstruction for a given day. Conventional sequential assimilation approaches used operationally make no use of "future" data outside the window of current data analyzed for forecasting. Here we introduce a new approach for application to large global ocean reanalysis systems that have only been run in "forward mode" (using past data), using the history of stored data increments to produce a more physically plausible time-evolving ocean state with smoother temporal adjustments toward the available observations.

1. Introduction

Ocean reanalysis products are now valuable sources for studying historical changes and variations in the ocean state and circulation (Balmaseda et al., 2015; Buizza et al., 2018; Jackson et al., 2016, 2019; Lea et al., 2006; Uotila et al., 2018). Reanalyses for both the atmosphere and oceans are normally produced using the same codes as are used for initializing short term numerical weather predictions (NWP) and ocean forecasts, or seasonal weather forecasts. Longer timescale decadal forecasts (e.g., Smith et al., 2007), have also been developed based on initializing with ocean reanalysis products. The sequential assimilation systems used for real-time forecasting regularly combine model output containing the history of previously assimilated data, together with recently acquired new observations to create a current ocean analysis from which new forecast computations can begin. In a reanalysis the "re-" reflects the production of a uniform sequence of analyses over a historic period, all performed with the same model and assimilation system, including uniformly reprocessed input data, boundary conditions, and forcing fields, which is not the case for the original analyses produced for real-time forecasts because of real-time data availability and the forecast systems themselves being regularly upgraded.

Such approaches work well for the atmosphere where observations are dense, both spatially and temporally, memory timescales are short and the daily analysis cycles used for numerical weather forecasts capture all the relevant information during a reanalysis. However the ocean observing system is more sparse, and only recently established, and the oceans may exhibit longer memory timescales than the atmosphere, especially below the surface. This means that an ocean reanalysis could seek to use more "future data," especially from locations not observed in the recent past, to help produce the best state estimation on a given day. Conventional sequential assimilation approaches used for ocean forecasting are not making of these "future" data outside the forward

assimilation window, which could substantially improve the historical reconstructions. A second problem with sequential analysis systems is that they are sensitive to the sudden introduction of new data as it becomes available, especially for the inhomogeneous *in situ* observing system we have for the subsurface oceans. This can lead to discontinuous changes in analyzed properties such as ocean heat content, as data are assimilated. These sudden discontinuities may be problematic for using reanalysis timeseries for following climate signals in the oceans, and for trying to infer information about processes that are not being properly represented by the models.

One approach to overcome these problems is to use the 4DVar assimilation approach (e.g., Powell et al., 2008; Smith et al., 2015). However there are fundamental problems with running 4DVar over extended time periods for chaotic systems such as the oceans. The ECCO consortium has overcome many problems with sustained efforts (Forget et al., 2015; Heimbach et al., 2019; Wunsch et al., 2009). However there are also many technical challenges in developing 4DVar methods for large models, especially the need for an adjoint code which must be continuously updated along with the ocean model, and therefore very few working 4DVar systems exist for realistic global ocean models used for operational forecasting, although some 4DVar regional ocean systems do exist (e.g., Lee et al., 2018).

Alternatively, Kalman smoothers (Anderson & Moore, 1979; Carrassi et al., 2017; Fukumori, 2002; Menard & Daley, 1996), should be able to produce optimal 4D analyses for linear systems. Ensemble Kalman filtering (Evensen 1994, 2003), has been well explored for approximating optimal sequential filtering for nonlinear large systems and is already commonly used for large operational systems (Houtekamer et al., 2014; Miyoshi et al., 2010). These ideas have also been extended theoretically to Ensemble Kalman Smoothers (Bocquet & Sakov, 2014; Evensen, 2018; Evensen & van Leeuwen, 2000), however there has been far less work applying optimal smoothing for large nonlinear systems such as ocean reanalyses (Cosme et al., 2010, 2012; Evensen, 2018; Evensen et al., 2019).

Conventional Kalman smoothing algorithms seek to propagate data backwards in time using the dynamical system itself as a propagator. This can be done in a single step for all time for a linear system (e.g., Aravkin et al., 2017), or for a nonlinear system an iterative technique can be used as in the outer loop of a 4DVar algorithm (e.g., Fisher & Auvinen, 2011). These methods are computationally expensive and are not generally used in high resolution models such as those in operational oceanography. However the sparsity of the ocean observing system coupled with the slower evolution compared to the atmosphere (making geolocated data useful *in situ* for longer) combine to make it realistic to consider the simpler problem of bringing future increment information into use during a reanalysis without substantial modification from a dynamical propagation step.

In this paper we introduce a new approach to the smoother problem for application to large global ocean reanalysis systems. The aim is not necessarily an optimal reanalysis, but one that produces a more physically plausible time-evolving ocean state with smoother adjustments towards available observations. Section 2 describes a sequential data assimilation (DA) test system using the Lorenz 1963 model and also the ocean model and sequential DA problem we are seeking to smooth based on the current Met Office operational Forecasting Ocean Assimilation Model (FOAM). Section 3 describes the smoother algorithm along with a brief discussion of its relationship to more optimal Kalman smoothing approaches. Section 4 shows results of applying the approach to a twin experiment with the Lorenz 1963 model. Section 5 describes the results obtained from applying the smoother to the FOAM system, looking at both RMS errors of the smoother fields against observations and smoothed climate metrics. Section 6 describes the improvements in time evolution of ocean states. Section 7 discusses potential applications of such smoother results, and Section 8 gives a summary and conclusions.

2. The Model Frameworks

2.1. The Lorenz 1963 Twin

To test out our new smoother we have set up an identical twin experiment with the Lorenz (1963) model. The "truth" run is performed over a period of 2,000 timesteps with a timestep of 0.01, starting with values of 5 for the x, y, and z variables. Observations are taken with an x observation frequency of 20 timesteps and a y observation frequency of 100 timesteps (and no z observations). An observation error standard deviation of 2 is applied to all observations. A time window of 5 timesteps together is used as the assimilation window in which a 3DVar FGAT approach is applied (see Section 2.2) where static background error covariances between x, y, and z allow increments to be applied to non-observed variables. The separation between observations means there are windows

during which no current observations are available in the forward run, however the smoother will allow future observations to still be applied. A 100-member ensemble of such assimilation experiments are performed, each starting from different initial conditions.

2.2. The Met Office FOAM System

For the ocean we have worked with the Met Office FOAM version 14 used by the Met Office for Met Ocean predictions (Blockley et al., 2014), and for initializing the ocean component of coupled seasonal forecasts. The ocean model is the GO6 version of NEMO (Madec, 2008; Madec & the NEMO Team, 2012) at global ¼° resolution on the ORCA025 grid, as described in Storkey et al. (2018). The assimilation method is NEMOVAR which uses a sequential 3DVar FGAT (First Guess at Appropriate Time; e.g., Lorenc & Rawlins, 2005) approach, assimilating data on a daily basis (Mirouze et al., 2016; Waters et al., 2015). The observations assimilated include altimeter sea level anomaly data, *in situ* temperature and salinity profile data from Argo and other platforms, sea surface temperature data from satellite and *in situ* platforms, and satellite-derived sea ice concentration data (Waters et al., 2015).

The 3DVar FGAT approach as used at the Met Office involves a 1-day *background run* of the model without data assimilation, during which the model counterparts of the observations are calculated at the nearest model timestep to the observation times. The observation space discrepancies (called the *innovations*) are then fed into the NEMOVAR code which uses observation and background error covariance estimates to statistically derive a 3D distribution of *assimilation increments* in temperature (T), salinity (S), sea surface height (SSH), velocity (U and V) and sea ice concentration for that day. A second *analysis run* of the model is then performed while adding these increments equally distributed throughout the day, as an incremental analysis update (IAU; Bloom et al., 1996). We note that the 1-day time mean fields from this analysis run are archived which, as well as representing a 1 day smoothing, also means that only ½ the NEMOVAR increment has been added for each days' analysis, which can be corrected for along with the smoothing operation.

The FOAM model is initialized daily for operational oceanography and is forced with atmospheric NWP model forecasts from the Met Office Unified Model in order to provide real-time predictions of the ocean state. In the experiments performed here the FOAM model is run in reanalysis mode although still using Unified Model NWP fluxes. For a full reanalysis an ERA atmospheric reanalysis can be used to drive the model at the surface more consistently over a long period.

The results reported here are based on the FOAM model analysis for the short period June–August 2016. During this period there are analyzed model fields of T, S, U, V, and SSH available as daily mean output data centered at 12:00 UTC. Also available are the assimilation increments that have been calculated by the NEMOVAR code and are added each day during the IAU run of the model which produces the final analysis. Thus each analyzed daily field contains information from the increments based on observations on all previous days but has no information about future increments. It is on this basis that the smoother algorithms described in the following section have been developed.

3. Smoother Algorithm

The reanalysis problem is similar to a fixed-interval smoother (Anderson & Moore, 1979). The Kalman smoother works with the innovations in observation space and attempts to calculate a set of smoother increments based on future innovations (e.g., Cosme et al., 2010, Equation 4b), by developing error covariances linking forecast (background) and analysis errors across time. An infrastructure for calculating full state space increments from innovations therefore needs to be in place to run a Kalman smoother, which requires further runs of the model and/or extensive storage of covariance distributions for projecting information between variables across space and time. Here we will develop a simpler smoothing approach based on using only the future sequential *forward model increments*, rather than *future innovations*, making the approach very much easier to run. The important difference with the Kalman smoother is that spatial and inter-variable error covariances are taken directly from model and observation errors available during the forward analysis cycle only, with a simple decay time used to reduce those covariances backwards in time. The main disadvantage is that there is no attempt to use the model, or a model adjoint, to project future innovations back into increments at earlier times based on the flow. However this smoother will still account very effectively for observations made in new regions which were not available

at all in the forward pass, and also where the system evolution is relatively slow so that error covariances do not evolve rapidly (Haines et al., 2006; Troccoli & Haines, 1999). This can be very useful in the ocean, especially below the surface, where *in situ* observations are sparse and inhomogeneously distributed in space and time. Here increments calculated by the sequential 3DVar code are brought backwards in time while reducing their amplitude based on their remoteness from the observation time.

We define A_t to be the original forward analyzed field during analysis window t, and I_t to be the increment field applied during this window used to produce A_t. We also define $\gamma < 1$ as the increment decay rate per assimilation window and note that this could be chosen to vary spatially or to be different for different variables if required. The smoother solution in window t is denoted S_t. The basic smoother algorithm can then be written;

$$S_0 = A_0 + \gamma(I_1) + \gamma^2(I_2) + \gamma^3(I_3) + \gamma^4(I_4) + \ldots\ldots; \tag{1}$$

so that increments from future windows ($t > 0$) decay by a factor γ per assimilation window in their influence on S_0. Similarly we can write;

$$S_1 = A_1 + \gamma(I_2) + \gamma^2(I_3) + \gamma^3(I_4) + \gamma^4(I_5) + \ldots\ldots; \tag{2}$$

and by rearrangement we can find

$$S_0 = A_0 + \gamma(S_1 - A_1 + I_1) = A_0 + SI_0, \tag{3}$$

and

$$SI_0 = \gamma(SI_1 + I_1), \tag{4}$$

where $SI_t = S_t - A_t$ is the "***smoother increment***." This recursive relationship allows the smoother to be run backwards in time starting with the final analyzed time window tf, and with $SI_{tf} = 0$ (there being no future increments).

The decay timescale τ (in assimilation window units) associated with the smoothing can be defined by the relationship;

$$\gamma^\tau = \frac{1}{e} \;\; or \;\; \tau = -\frac{1}{\ln(\gamma)} \tag{5}$$

Another insightful quantity is the total number, NS, of whole future assimilation increments contributing to each smoother increment SI;

$$NS = \frac{\gamma}{1-\gamma} \tag{6}$$

So for example $\gamma = 0.7$ corresponds to a decay timescale $\tau \sim 3$ windows, with $NS \sim 2.3$ future window increments contributing to each smoother increment, and $\gamma = 0.98$ would correspond to $\tau \sim 50$ windows and $NS = 49$ future window increments.

4. Smoother for the Lorenz 1963 System

The Lorenz (1963) system described in Section 2.1 was run over 20 time units to create the "truth" run. The 100-member analysis ensemble, each starting from different initial conditions, but otherwise with the model unchanged, was run with observations of x and y, with their errors, assimilated and analysis increments stored. Then the smoother increments were calculated for each assimilation window, as described in Section 3, using a smoother parameter $\gamma = 0.7$. The success of the analysis and smoother results were assessed as RMSE against the truth.

Figures 1a, 1b, 1d and 1e show the x, y timeseries and the applied increments for a single assimilation run. Notably the analysis increments (red, *b, e*) are confined to the windows where observations are made, only influencing the subsequent analysis, while the smoother increments (green) spread backward, with decay, over the windows between observation times. Note that the smoother increments are added offline on top of the original filter increments. Figures 1c and 1f show the x, y RMSE against truth timeseries for the 100-member ensemble. The
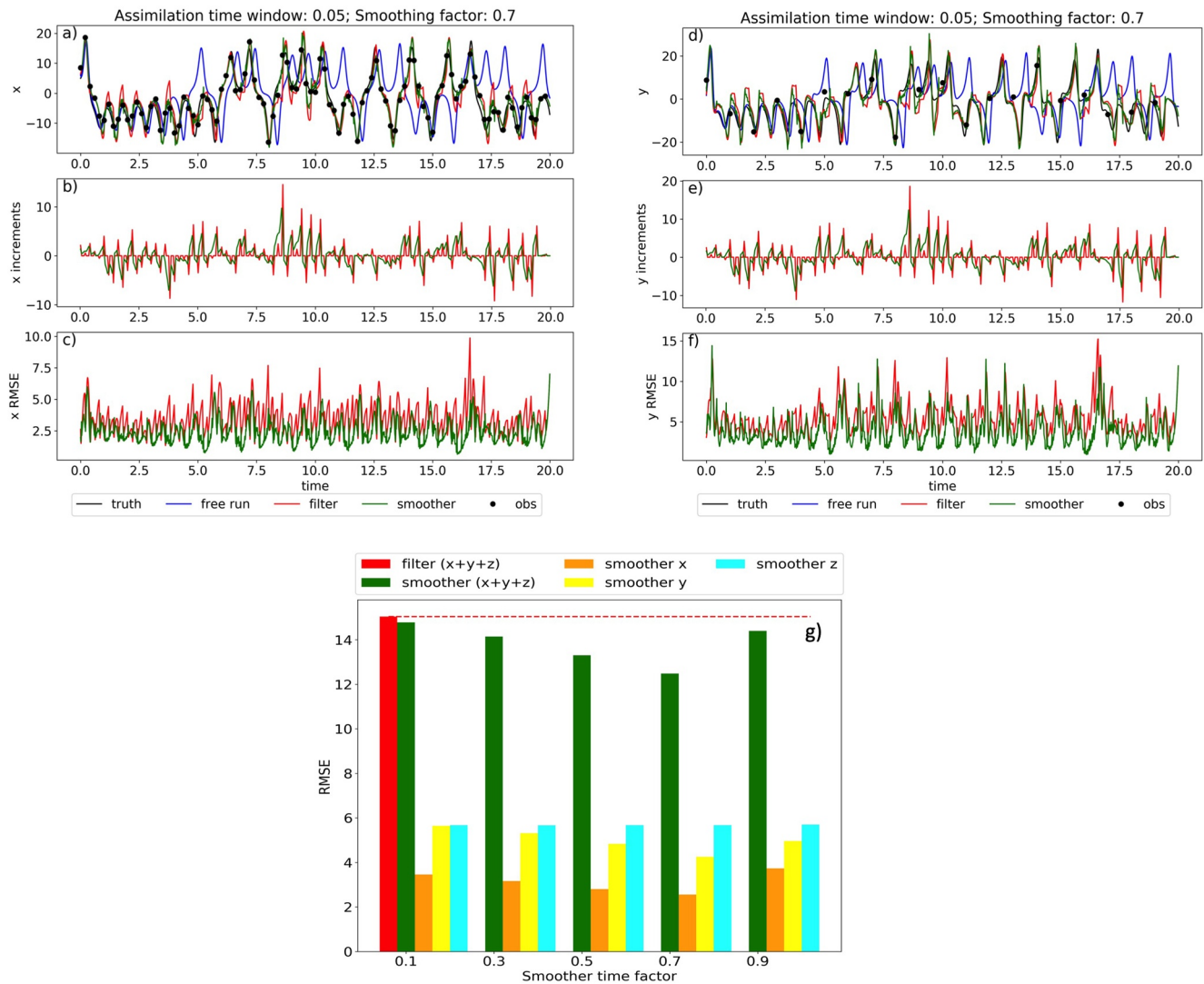
Figure 1. Lorenz 1963 truth, background (free run), analysis (filter) and smoother results. (a) *x* timeseries for a single ensemble member, with dotted observations, (b) same member's *x* increments for analysis (red) and the smoother (SI_t, green), (c) *x* ensemble RMSE timeseries for analyses (red) and smoothers (green). Panels (d, e, and f) show the same for the *y* variable. Panel (g) shows the average ensemble mean RMSE for *x, y, z*, and the sum, for the analysis and smoother, with variations in the smoothing parameter γ.

substantial reductions in error between observation times for the smoother are clear, where these represent errors against independent data (no observations are available during these periods). This distinction will be useful for the later FOAM results. The *z* timeseries are not shown as no significant impacts occur.

The time averaged RMSE for the smoother ensemble (Figure 1g) is clearly reduced compared with the analysis for both *x* and *y*, with the largest reduction for the more sparsely observed *y* variable. The smoother reduces the errors compared to the filter over a wide range of γ values, with the largest reductions occurring with $\gamma = 0.7$, as used for the single member smoother (Figures 1a, 1b, 1d and 1e). These results clearly demonstrate the practical effectiveness of the simple smoother algorithm.

5. Smoother Results for the Met Office FOAM System

5.1. Implementation for FOAM

As noted in Section 2.2 the archived FOAM fields are averages over the IAU window and therefore only contain ½ the current increment, therefore to be consistent as we begin to add future increments, an additional ½ increment for the current timestep is added to the smoother fields described in Section 3.

The smoother parameter selected for the whole domain was $\gamma = 0.7$ giving a decay timescale $\tau \sim 3$ days with the 1 day assimilation windows used by FOAM. This is regarded as a very realistic timescale at the ocean surface (Tanimoto et al., 1993) and is around the timescale used during the analysis of satellite sea surface temperature data when it is being combined into an analyzed SST product (Roberts-Jones et al., 2016). We did experiments with much longer timescales for the subsurface ocean, for example, if $\gamma = 0.98$ this corresponds to $\tau \sim 50$ days, broadly consistent with correlation timescales for deep water properties (e.g., Johnson et al., 2015). However the number of whole assimilation increments then contributing to the smoother increment is $NS = 49$ leading to problems of assimilation bias. If the increments are being even partially rejected by the ocean model in the sequential forward analysis run then the same or similar increments can appear again and again as the subsequent observations try to insert the same correction that the model will not retain. Such bias corrections may only be a minor inconvenience during the original forward analysis, but in the smoother algorithm used here such bias increments would reinforce NS times leading to large erroneous changes.

It may be possible to correct for bias in the recursive smoothing algorithm if the bias, b, can be correctly identified ($I => I-b$ in Equations 3 and 4) however this is not an easy thing to do with the inhomogeneous space-time observations available in the subsurface ocean. We performed a number of experiments using longer smoothing times in the ocean subsurface using different ways of determining bias however these results are left as further work. Here results are presented using the same short timescale based on $\gamma = 0.7$, and on these short timescales bias correction is unnecessary nearly everywhere.

The smoother algorithm is only run on the T and S fields. The velocity and sea level field increments must satisfy closely geostrophic relationships with the density field increments and the smoothed versions of these can be found using balancing operators, as is performed in the normal course of assimilation (Mogensen et al., 2012). The thermal wind balance is applied directly to the smoothed density increments using a dynamic level of no motion change at 1,500 m depth, as is done for the forward run assimilation increments (Weaver et al., 2005). This results in a balanced smoother increment for the sea surface height and velocity fields which can be added to the original analysis fields.

5.2. Errors Against Observations

In what follows we mostly show error diagnostics of the T, S, SSH model fields against the observations, based on standard diagnostics output by the operational DA system. These are calculated in observation space and then averaged into $5 \times 5°$ boxes and over the top 2,000 m, for a single month, June 2016. Comparisons are made for the original analysis run in forward mode and for the smoother solution after the additional smoother increments have been incorporated. Each model product has been interpolated to the locations of the observations.

Figure 2 shows the mean temperature bias for June 2016, where Figure 2a is for the original *analysis* run after data assimilation. The observations being compared against have now been assimilated but the *analysis* fields still show differences based on the relative weights given to the background and the data. Figure 2b shows the *smoother* run results. Figures 2c and 2d are the equivalent temperature RMS differences against the observations for the top 2,000 m.

It can be seen that the smoother differences, for both mean error (or bias) and RMS, are substantially smaller than those of the analysis in virtually all regions, in the central ocean basins as well as in areas of strong currents near boundaries and even in the southern ocean. However the existence of the mean bias does indicate the places where potential problems start to arise as NS becomes large if longer smoothing timescales are implemented, as discussed above. Figures 3a–3d are the same set as Figures 2a–2d except that the bias and RMS differences are shown for salinity through the top 2,000 m. The RMS salinities are much larger than the bias now, but the
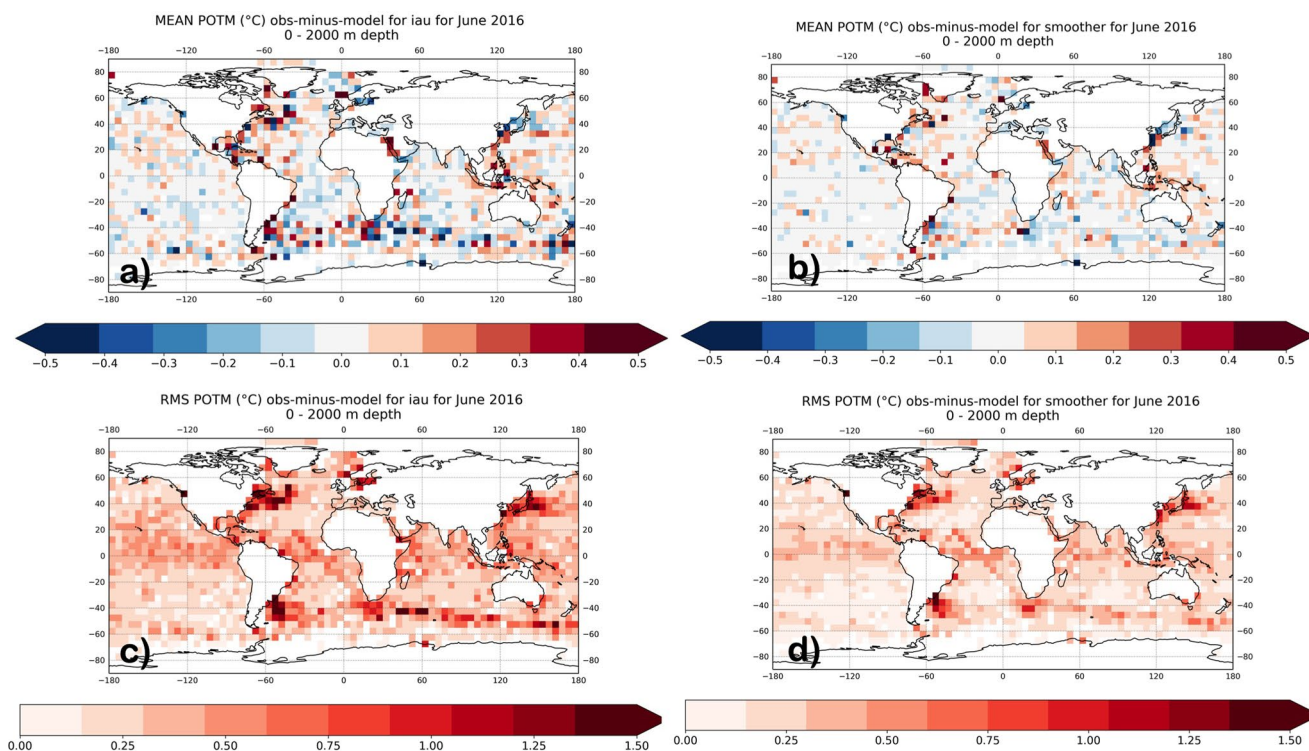
Figure 2. (a) Mean temperature (°C) difference of *analysis* against daily observations for top 2,000 m. (b) Mean temperature difference of *smoother* against daily observations. (c) RMS temperature difference of *analysis* against daily observations. (d) RMS temperature difference of *smoother* against daily observations. All error diagnostics are based on data in June 2016.
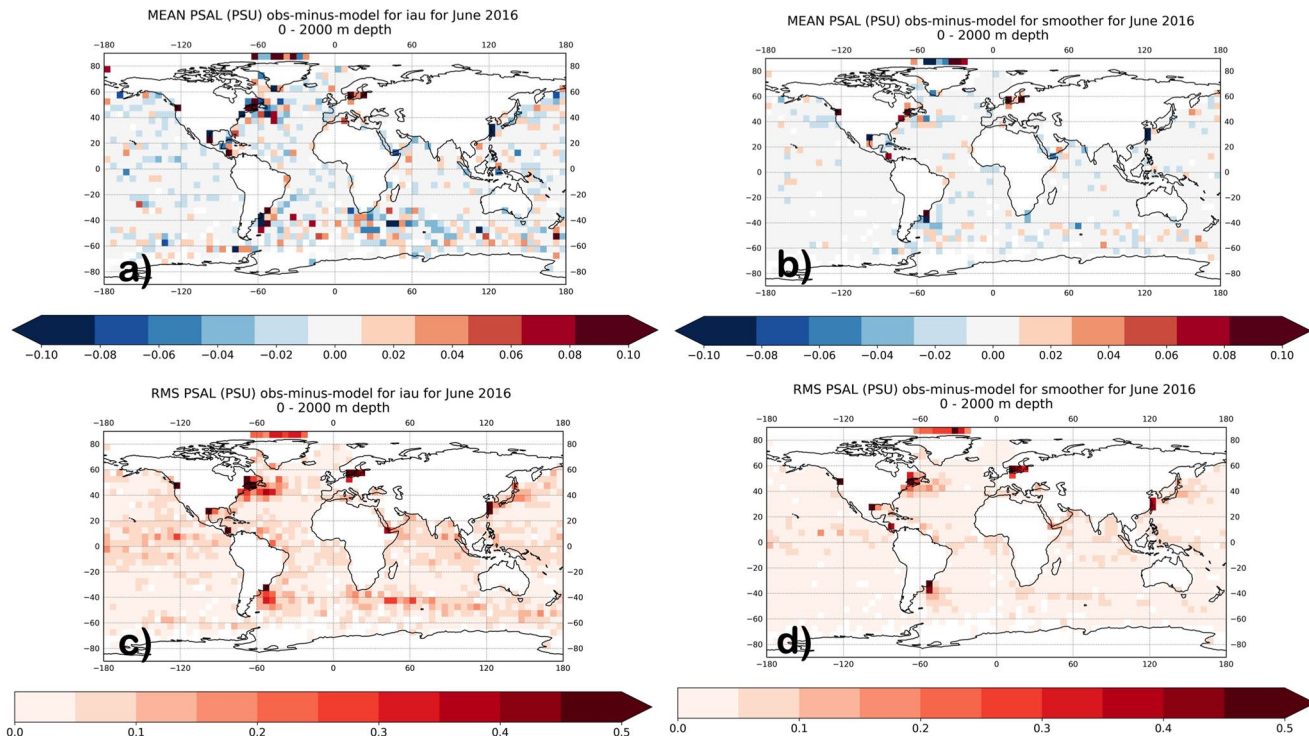

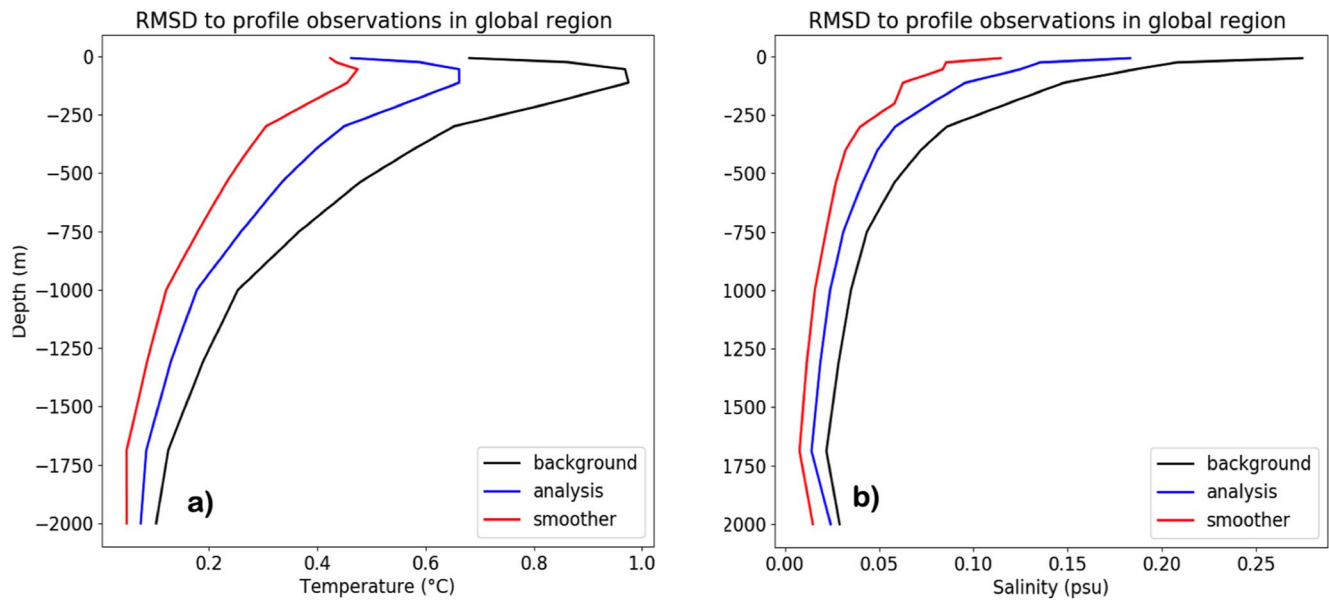**Figure 3.** As in Figure 2 but for salinity (PSU) differences.

Figure 4. (a) Global average RMS errors in temperature (°C) as a function of depth for the *background* (1-day forecast) fields (black), the *analysis* fields (blue), and the *smoother* fields (red). (b) As in (a) but for salinity (PSU).

smoother results make an even more striking improvement. Again all regions are being improved to some extent by the smoother process.

Figures 4a and 4b show the global depth profiles of the temperature and salinity differences against observations, respectively. In this case each plot has 3 lines showing the background RMS differences based on the 1-day forward model run performed prior to data assimilation, the analysis differences and the smoother differences through the top 2,000 m. It is clear that the ocean smoother results have substantially lowered errors for both T and S in all depth ranges. The error reductions between analysis and smoother is similar to the reduction between background and analysis.

Figure 5a shows the RMS sea surface height errors for the analysis run on a 5 × 5° grid. As noted above the sea surface height smoother increments are based on a dynamic height calculation using the T and S smoother increments and the observations being compared with are the altimeter data. Figure 5b shows the percentage reduction in these RMS SSH errors for the smoother solution, defined as 100 × (Analysis RMS–Smoother RMS)/ Analysis RMS. Again the smoother solution is seen to be considerably closer to observations than the analysis in all regions, as demonstrated by the reduction in RMS differences.

There is an important caveat to the above results. (a) The FOAM smoother results have added an additional ½ increment from the current data to account for the daily IAU run averaging used in the archived analysis. This means that the smoother solution is being directly moved toward the current observational data due to this component alone, irrespective of any future window data. (b) Being closer to the observational data each day is of course no guarantee of an overall improved product. This could be achieved in the forward model simply by increasing the background error, however this can lead to overfitting the observations, which will themselves have errors. A comparison against independent (unassimilated) observations would be preferable, as achieved for the Lorenz 1963 model in Figure 1.

To address point (a), Figure 5c shows the percentage reduction in SSH RMS errors for the smoother when the ½ increment from the current analysis time is not included. In this case the solution is only using the future smoother increments, Equations 3 and 4 to update the analysis. It can be seen that in the strong current regions where SSH and current variability is most rapid, for example, the Gulf Stream, Kuroshio and Southern Ocean, there are still substantial reductions in SSH errors based on smoothing in future data. Elsewhere the smoother impact is very small or slightly negative. If T and S RMS errors are examined in these same high variability regions they are also improved by future observations alone although results are noisy and harder to show as maps, and elsewhere the impacts are small or slightly negative as for the SSH.
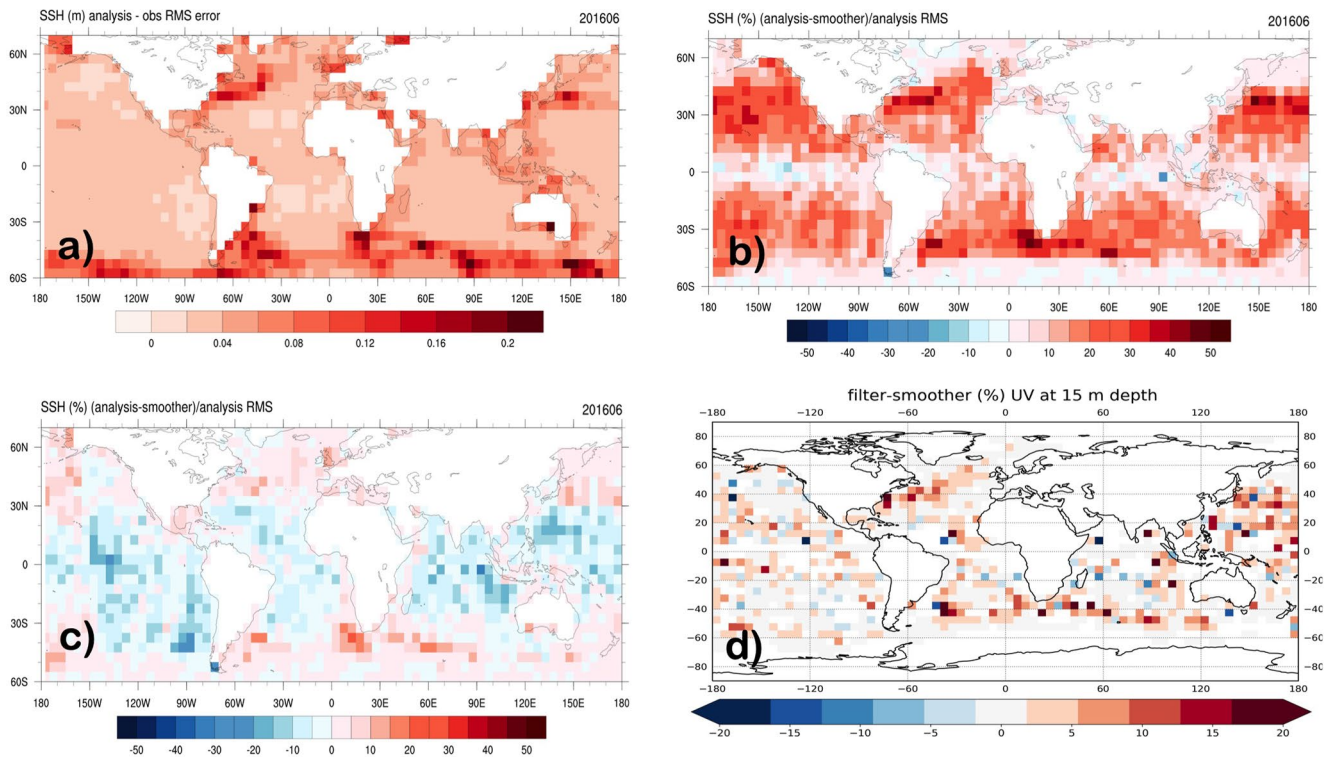
Figure 5. (a) *Analysis* RMS SSH errors (in unit of m) against daily altimeter observations. (b) Percentage reduction in *smoother* RMS SSH compared to *analysis* (a). (c) As (b) for *smoother* with "future increments only" included. (d) Percentage reduction in "future increment only" *smoother* U, V (15 m) RMS differences against drifter measurements compared to U, V RMS for the *analysis*. Panels (b–d) are shown as 100% × (Analysis RMS-Smoother RMS)/Analysis RMS so that positive (negative) values indicate that the *smoother* has smaller (larger) errors.

To address point (b), Figure 5d shows near surface (15 m) U and V current RMS errors, compared against independent U, V data from drifters in observation space. We used the unfiltered estimates of the zonal and meridional velocities at 15 m depth measured by drifting buoys produced by the Copernicus Marine in situ TAC (2020) and compared these to the 15 m depth filter and smoother velocities. These drifter trajectory data have not been assimilated and are indeed in quite different time and space locations to the altimeter data, which provide most of the relevant information on near surface currents. The figure shows the percentage error reduction given by the smoother over the analysis, defined as 100 × (Analysis RMS–Smoother RMS)/Analysis RMS, averaged in 5 × 5° boxes for June 2016. It is clear that the smoother results represent a significant improvement over most of the ocean domain and particularly in areas of strong current variability.

These comparisons against observations strongly suggest that the application of the smoother increments is improving on the analyzed fields and that future data provide improvement especially in the regions of strong variability. These results, along with the idealized results in the Lorenz system (Figure 1), give some confidence that the smoother results constitute a significant improvement over the analysis. We believe this is especially the case in places where near future observations are present but past observations are not. An additional aim of the smoother is to improve the temporal evolution of the analysis by allowing the smoother introduction of observations which are significantly correlated in time. In the next section we will look at the temporal smoothing aspects of the solution, smoothing out some of the large adjustments to ocean state fields which are introduced through the daily sequential analysis.

6. Smoothed Ocean Time Series

6.1. Heat and Salt Content

The ocean heat content (OHC) 0–2,000 m from the original FOAM *analysis* in the subtropical region 26–45°N in the North Atlantic over the short period June-August 2016, is shown in the black line in Figure 6a. The strong
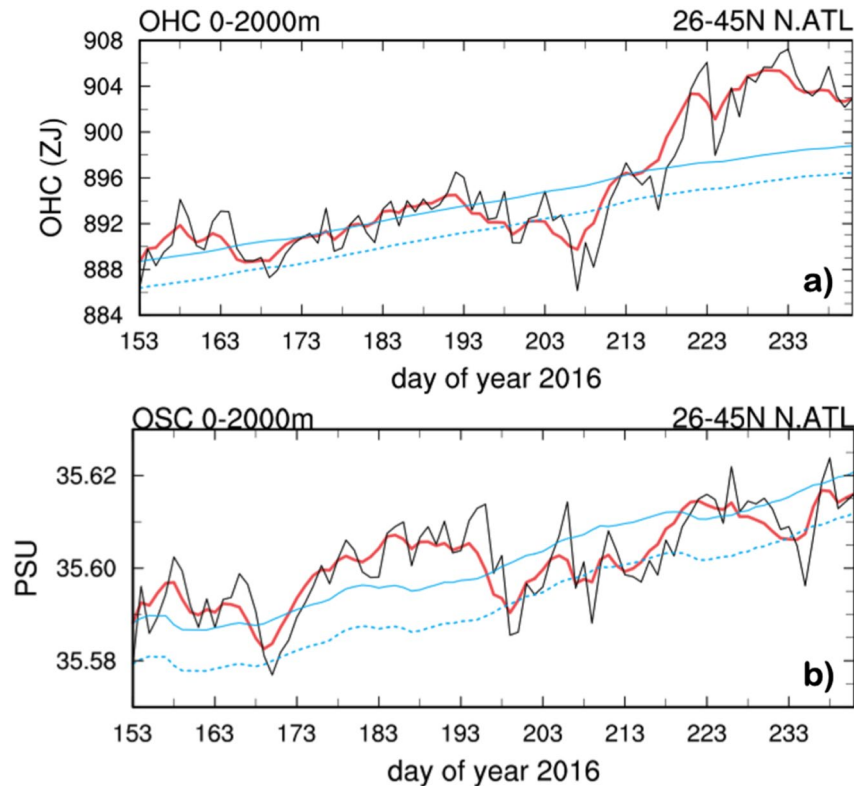
Figure 6. 0–2,000 m OHC time series averaged over 26–45°N Atlantic Ocean for June–August 2016. Red line is the *smoother* output, black line is from FOAM *analysis* and blue dashed line is the reconstructed *free* model evolution. The solid blue line is the *free* run starting from the same OHC as the *smoother* result. (b) As (a) but for OSC.

high frequency variability has a comparatively large amplitude compared to the slow evolution of OHC on a monthly timescale, and is being driven by assimilation of data which is highly irregular in space and time. We do not have a truly free model run to demonstrate this, but we can generate an artificial free evolution using OHC 1-day tendencies from the *background* runs made during DA. The dashed blue line in Figure 6a is obtained by stringing together all the 1-day OHC *background* tendencies starting from the analysis initial conditions on June 1. It can be seen that these *background* run changes in OHC over this large area are small and smoothly varying each day, and therefore clearly all the high frequency changes taking place in the *analysis* run are coming directly from the DA. We can also rule out transport of heat as contributing to the higher *analysis* OHC variability, as *analysis* transports will also be present in the "free run." These high frequency OHC variations can mask any lower frequency changes which might represent realistic information on OHC coming from the assimilated data.

The red line in Figure 6a shows the new smoothed reanalysis evolution based on Equation 3. The smoothing operation has removed some of the high frequency variability in the original analysis timeseries by bringing forward future increments. The smoother analysis and the background-based free model run are displaced with respect to each other mainly because the free run starts from the start of the analysis run, while the smoother starts from the end point of the analysis. The solid blue line shows the "free model" evolution displaced to match the first day of the smoother solution. The two solutions are now more similar although analysis over a longer time period may reveal realistic differences associated with assimilation of the data which may be harder to detect from the original analysis with its higher frequency variability. Figure 6b shows the ocean salt content (OSC) over the same region as Figure 6a, and the smoother evolution of the salt content is very clear.

Figures 7a and 7b show the original and smoother analyses for OHC for two additional regions, in the Equatorial Pacific (5°S–5°N, 170–120°W) and in the Antarctic Circumpolar Current (ACC, 50–60°S, 130–170°E) regions. Figures 7c and 7d show the OSC for these Equatorial and ACC regions. In the Equatorial Pacific, the daily variability in the analysis is relatively small and so the smoothed reanalysis shows a smaller effect on both OHC and
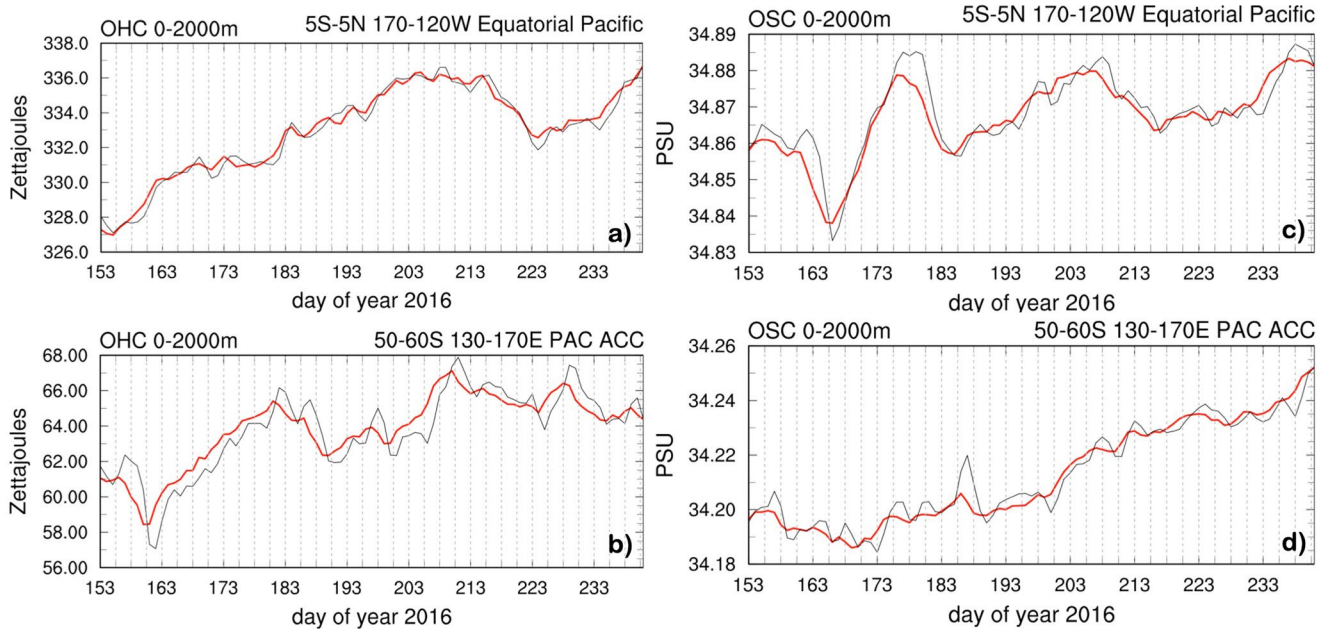
Figure 7. (a) *Smoother* (red line) and *analysis* (black line) 0–2,000 m OHC timeseries for Equatorial Pacific 5°S–5°N, 170–120°W for June–August 2016. (b) OHC timeseries for ACC region 50–60°S, 130–170°E. (c) OSC timeseries as in (a). (d) OSC timeseries as in (b).

OSC than in the subtropics and ACC regions. The results in each of these different regions clearly show smoother and more realistic OHC and OSC time evolution than the original unsmoothed analysis.

6.2. Turbulent Kinetic Energy (TKE) and the AMOC

Figure 8 shows the original and smoother analyses for 0–1,000 m turbulent kinetic energy (TKE) for the 26–45°N Atlantic region. The smoothed TKE shows a very slight increase in mean TKE over the original analysis over the 3 months period, but significantly reduced high frequency variability and therefore a smoother evolution on weekly to monthly time scales. This shows that the time variability in the velocity field is also being smoothed and is likely to be more realistic, benefiting from assimilating future data over a wider domain. There will be an unbalanced (ageostrophic) component of the velocity field which is not being improved by the smoother, including inertial wave motions, some of which are excited by the data assimilation process itself (Blaker et al., 2021; Fox et al., 2000).
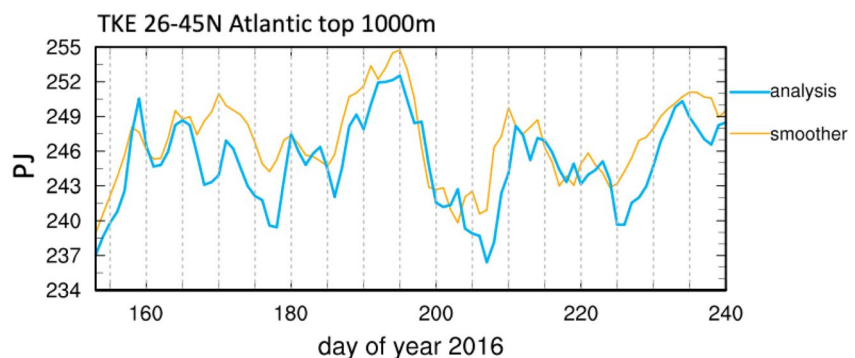

Figure 8. (a) *Smoother* (orange line) and original *analysis* (blue line) time series of 0–1,000 m turbulent kinetic energy (TKE, in unit of petajoules) averaged over 26–45°N Atlantic Ocean for June-August 2016.
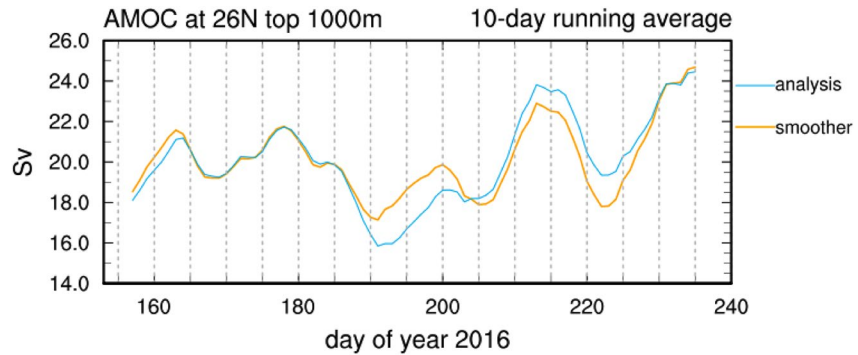
Figure 9. *Smoother* (orange line) and *analysis* (blue line) AMOC (in unit of *Sv*) 10-day running average time series at 26°N.

Figure 9 shows the Atlantic Meridional Overturning Circulation (AMOC) at 26°N for the original and smoother analyses. We show both as 10-day running means because higher frequency AMOC variability cannot in any case be monitored (McCarthy et al., 2015) and would be of little importance for heat transport or climate variability. The smoother result clearly shows reduced temporal variability with largest peak to peak changes reduced by 4 *Sv* compared with the analysis on week to month timescales. This indicates that the smoother does have a potentially detectable impact on important aspects of oceanic transports.

7. Discussion

The Lorenz model analysis allows additional tests to be made by varying observational sampling, observational error amplitudes, as well as different smoothing timescales (Figure 1g), although it cannot really replicate long memory timescales associated with conserved properties in the ocean. When the smoother solution is compared only with the truth at times when observations are assimilated, more similar to comparisons with observations in the FOAM system, then errors are improved considerably less than is shown in Figure 1, showing that it is the unobserved periods between observation times that benefit the most. We would expect the same to be the case in the ocean model.

It should also be noted that an optimal Kalman smoother should not need an externally defined smoothing timescale because the temporal smoothing of different signals should depend on physically modeled processes. However the specified smoothing timescales we use still makes physical sense when considered as a smoothing of data into the gaps between observation times. From this perspective the smoothing timescale of a few days fits reasonably well with the repeat timescale for altimeter observations or the surfacing cycle of Argo floats, both around 10 days (Rio et al., 2014).

Although the largest RMS error reductions against observations, compared with the daily average analyses, occur through completing the addition of the current data increment, we find that significant improvements in errors also occur through use of future increments in the areas of strong variability where the mesoscale signal is larger and arguably more dominant over any observational errors. These future increments are then independent of the current observations and therefore provide a strong test of the consistency and value of the smoothing. Perhaps most impressive is the improvements of the smoother against fully independent drifter U, V currents, again especially in areas of strong currents. This suggests that significant improvements to the mesoscale fields can be obtained by smoothing.

Turning to the timeseries, other approaches can be used to give smoother OHC signals such as simply temporally smoothing the original analysis but this leads to smoothing the model background as well as the increments, which is undesirable especially during events generated by high frequency forcing, for example, tropical storms. The *in situ* observations alone can be used to give a low frequency estimate of OHC variability (Abraham et al., 2013) but space-time interpolation scales are still required and no use is then being made of the dynamics captured by an ocean model to propagate past observations forward in time, or of the high quality atmospheric reanalysis data which can generate realistic ocean variability, in the reconstructions. Formally a full 4DVar approach with an

ocean model might be preferable but this is computationally expensive and hard to perform for high resolution state-of-the-art operational models (e.g., Lea et al., 2006). It is also interesting to consider whether instead of simply applying the smoother increments offline as here, the method could be iterated with further reanalysis forward passes performed while giving some weights to smoother increments from the previous iteration.

One possible application of this work would be a better assessment of the ocean heat and salt content of a region around which budget studies are to be performed. The strong sensitivity to the data assimilation makes it hard to distinguish realistic OHC change signals present in the original analysis. As for the OHC itself there is evidence that ocean volume and heat transports from standard sequential reanalyses have more variability than free running ocean or coupled models, and that much of this variability may represent noise introduced by data assimilation (Karspeck et al., 2017; Meinen et al., 2010; Zhu et al., 2012). Overall the simple smoother approach should provide more consistent OHC and OSC estimates based on observations using all available data and dynamical understanding. There is also every reason to expect that a smoother introduction of assimilated data, would reduce noise in ocean transports obtained from reanalyses, as seen from the smoother AMOC timeseries in Figure 9, and so allow for more reliable assessment of heat or freshwater transport variability for use in regional ocean budget studies.

8. Conclusions and Future Work

This paper has developed and tested a simple smoother algorithm that can be easily used with the most sophisticated operational ocean models. It takes advantage of the increment diagnostics that are regularly archived at operational oceanography centers such as the Met Office, Mercator Ocean and ECMWF, to perform the smoothing, as well as the "Class 4" observation space error diagnostics (Ryan et al., 2015), to demonstrate the performance of the smoother fields compared to observations.

The approach eschews the use of the model physical operator in bringing future observations back to influence earlier state estimates, and instead relies on a simple temporal decay time, which varies spatially, to generate the smoother increments. We first demonstrate the effectiveness of this simple approach using a Lorenz 1963 twin experiment and show that RMS errors against the known "truth" are reduced by the smoother, through adding increments in between observation times, based on the future observations coming more incrementally into the solution.

The smoother was then tested on a 3-month run of the Met Office global ¼°, 75-level FOAM operational ocean model, for diagnostics of ocean heat and salt content which are of great interest for understanding the global energy budget (von Schuckmann et al., 2018), as well as for regional heat and freshwater budget and transport studies (Douglass et al., 2010; Ganachaud & Wunsch, 2003). The smoothing is directly applied to ocean water properties of temperature and salinity, and smoother versions of the currents and SSH fields have been generated through geostrophic "balancing" adjustments. The smoother effectively removes high frequency variability in ocean heat and salt content in the reanalysis data that is generated by the sequential assimilation of sparse ocean observations, but without temporally smoothing the background ocean fields, giving a more realistic representation of the evolution of integrated ocean properties.

The smoothed fields were also compared directly to temperature and salinity profile data, and sea surface height data, with standard diagnostics used as part of the data assimilation process. The smoother results are additionally compared with entirely independent 15 m drifter velocities. It is found that the smoothed analyses are very significantly closer to the observations in both mean values and RMS errors at nearly all depth ranges and locations studied, including to the independent drifter results. The results presented here were obtained after only a limited amount of tuning of the smoothing timescales which were constrained to be short due to the presence of model bias in the operational analysis increments. Longer smoothing timescales could potentially be very useful in the pre-Argo period when *in situ* data are much more sparse. Further improvements could undoubtedly be obtained but this paper presents a first implementation of a new and very promising method that can easily be applied to ocean reanalyses from many operational centers using currently archived data, and which may improve their value for ocean and coupled process applications.

Data Availability Statement

Smoother reanalysis data for June 2016 are published at the CEDA Archive, http://dx.doi.org/10.5285/b0cf5a39647e4036bd5351274c5daa5f.

References

Abraham, J. P., Baringer, M., Bindoff, N. L., Boyer, T., Cheng, L. J., Church, J. A., et al. (2013). A review of global ocean temperature observations: Implications for ocean heat content estimates and climate change. *Reviews of Geophysics*, *51*(3), 450–483. https://doi.org/10.1002/rog.20022

Anderson, D., & Moore, J. (1979). *Optimal filtering. Information and system* (p. 379). Prentice-Hall, Inc.

Aravkin, A., Burke, J. V., Ljung, L., Lozano, A., & Pillonetto, G. (2017). Generalized Kalman smoothing: Modeling and algorithms. *Automatica*, *86*, 63–86. https://doi.org/10.1016/j.automatica.2017.08.011

Balmaseda, M. A., Hernandez, F., Storto, A., Palmer, M. D., Alves, O., Shi, L., et al. (2015). The ocean reanalyses intercomparison project (ORA-IP). *Journal of Operational Oceanography*, *8*(1), s80–s97. https://doi.org/10.1080/1755876x.2015.1022329

Blaker, A. T., Hirschi, J.-M., Bell, M. J., & Bokota, A. (2021). Wind-Driven oscillations in the meridional overturning circulation near the equator. Part I: Numerical models. *Journal of Physical Oceanography*, *51*(3), 645–661. https://doi.org/10.1175/JPO-D-19-0296.1

Blockley, E. W., Martin, M. J., McLaren, A. J., Ryan, A. G., Waters, J., Lea, D. J., et al. (2014). Recent development of the Met Office operational ocean forecasting system: An overview and assessment of the new global FOAM forecasts. *Geoscientific Model Development*, *7*, 2613–2618. https://doi.org/10.5194/gmd-7-2613-2014

Bloom, S. C., Takacs, L. L., Da Silva, A. M., & Ledvina, D. (1996). Data assimilation using incremental analysis updates. *Monthly Weather Review*, *124*, 1256–1271. https://doi.org/10.1175/1520-0493(1996)124<1256:dauiau>2.0.co;2

Bocquet, M., & Sakov, P. (2014). An iterative ensemble Kalman smoother. *Quarterly Journal of the Royal Meteorological Society*, *140*(682), 1521–1535. https://doi.org/10.1002/qj.2236

Buizza, R., Poli, P., Rixen, M., Alonso-Balmaseda, M., Bosilovich, M. G., Brönnimann, S., et al. (2018). Advancing global and regional reanalyses. *Bulletin of the American Meteorological Society*, *99*(8), ES139–ES144. https://doi.org/10.1175/BAMS-D-17-0312.1

Carrassi, A., Bocquet, M., Bertino, L., & Evensen, G. (2017). *Data assimilation in the geosciences: An overview of methods, issues, and perspectives*. https://doi.org/10.1002/wcc.535

Copernicus Marine in situ TAC. (2020). *Copernicus in situ NRT current product user manual (PUM)*. CMEMS-INS-PUM-013-048. https://doi.org/10.13155/73192

Cosme, E., Brankart, J.-M., Verron, J., Brasseur, P., & Krysta, M. (2010). Implementation of a reduced rank square-root smoother for high resolution ocean data assimilation. *Ocean Modelling*, *33*(1–2), 87–100. https://doi.org/10.1016/j.ocemod.2009.12.004

Cosme, E., Verron, J., Brasseur, P., Blum, J., & Auroux, D. (2012). Smoothing problems in a Bayesian framework and their linear Gaussian solutions. *Monthly Weather Review*, *140*, 683–695. https://doi.org/10.1175/mwr-d-10-05025.1

Douglass, E., Roemmich, D., & Stammer, D. (2010). Interannual variability in North Pacific heat and freshwater budgets. *Deep Sea Research Part II: Topical Studies in Oceanography*, *57*(13–14), 1127–1140. https://doi.org/10.1016/j.dsr2.2010.01.001

Evensen, G. (1994). Sequential data assimilation with a nonlinear quasi-geostrophic model using Monte Carlo methods to forecast error statistics. *Journal of Geophysical Research*, *99*, 10143–10162. https://doi.org/10.1029/94jc00572

Evensen, G. (2003). The ensemble Kalman filter: Theoretical formulation and practical implementation. *Ocean Dynamics*, *53*, 343–367. https://doi.org/10.1007/s10236-003-0036-9

Evensen, G. (2018). Analysis of iterative ensemble smoothers for solving inverse problems. *Computational Geosciences*, *22*, 885–908. https://doi.org/10.1007/s10596-018-9731-y

Evensen, G., Raanes, P. N., Stordal, A. S., & Hove, J. (2019). Efficient implementation of an iterative ensemble smoother for data assimilation and reservoir history matching. *Frontiers in Applied Mathematics and Statistics*, *5*, 47. https://doi.org/10.3389/fams.2019.00047

Evensen, G., & van Leeuwen, P. J. (2000). An ensemble Kalman smoother for nonlinear dynamics. *Monthly Weather Review*, *128*, 1852–1867. https://doi.org/10.1175/1520-0493(2000)128<1852:aeksfn>2.0.co;2

Fisher, M., & Auvinen, H. (2011). Long Window 4D-Var. In *Proceedings of the ECMWF Seminar Series on Data assimilation for atmosphere and ocean* (pp. 6–9).

Forget, G., Campin, J. M., Heimbach, P., Hill, C. N., Ponte, R. M., & Wunsch, C. (2015). ECCO version 4: An integrated framework for non-linear inverse modeling and global ocean state estimation. *Geoscientific Model Development*, *8*, 3071–3104. https://doi.org/10.5194/gmd-8-3071-2015

Fox, A. D., Haines, K., & De Cuevas, B. (2000). *Modelling internal waves with a global ocean model* (Vol. 39, pp. 27–30). WOCE Newsletter. Retrieved from https://eprints.soton.ac.uk/8869/

Fukumori, I. (2002). A partitioned Kalman filter and smoother. *Monthly Weather Review*, *130*, 1370–1383. https://doi.org/10.1175/1520-0493(2002)130<1370:apkfas>2.0.co;2

Ganachaud, A., & Wunsch, C. (2003). Large-scale ocean heat and freshwater transports during the World Ocean Circulation Experiment. *Journal of Climate*, *16*(4), 696–705. https://doi.org/10.1175/1520-0442(2003)016<0696:lsohaf>2.0.co;2

Haines, K., Blower, J. D., Drécourt, J. P., Liu, C., Vidard, A., Astin, I., & Zhou, X. (2006). Salinity assimilation using S (T): Covariance relationships. *Monthly Weather Review*, *134*(3), 759–771. https://doi.org/10.1175/mwr3089.1

Heimbach, P., Fukumori, I., Hill, C. N., Ponte, R. M., Stammer, D., Wunsch, C., et al. (2019). Putting it all together: Adding value to the global ocean and climate observing systems with complete self-consistent ocean state and parameter estimates. *Frontiers in Marine Science*, *6*, 55. https://doi.org/10.3389/fmars.2019.00055

Houtekamer, P. L., Deng, X., Mitchell, H. L., Baek, S. J., & Gagnon, N. (2014). Higher resolution in an operational ensemble Kalman filter. *Monthly Weather Review*, *142*(3), 1143–1162. https://doi.org/10.1175/mwr-d-13-00138.1

Jackson, L. C., Dubois, C., Forget, G., Haines, K., Harrison, M., Iovino, D., et al. (2019). The mean state and variability of the North Atlantic circulation: A perspective from ocean reanalyses. *Journal of Geophysical Research: Oceans*, *124*, 9141–9170. https://doi.org/10.1029/2019JC015210

Jackson, L. C., Peterson, K. A., Roberts, C. D., & Wood, R. A. (2016). Recent slowing of Atlantic overturning circulation as a recovery from earlier strengthening. *Nature Geoscience*, *9*, 518–522. https://doi.org/10.1038/ngeo2715

Johnson, G. C., Lyman, J. M., & Purkey, S. G. (2015). Informing deep Argo array design using Argo and full-depth hydrographic section data. *Journal of Atmospheric and Oceanic Technology*, *32*(11), 2187–2198. https://doi.org/10.1175/jtech-d-15-0139.1

Karspeck, A. R., Stammer, D., Kohl, A., Danabasoglu, G., Balmaseda, M., Smith, D. M., et al. (2017). Comparison of the Atlantic meridional overturning circulation between 1960 and 2007 in six ocean reanalysis products. *Climate Dynamics*, *49*, 957–982. https://doi.org/10.1007/s00382-015-2787-7

Lea, D. J., Haine, T. W., & Gasparovic, R. F. (2006). Observability of the Irminger Sea circulation using variational data assimilation. *Quarterly Journal of the Royal Meteorological Society*, *132*(618), 1545–1576. https://doi.org/10.1256/qj.05.77

Lee, J. H., Kim, T., Pang, I. C., & Moon, J. H. (2018). 4DVAR Data Assimilation with the Regional Ocean Modeling System (ROMS): Impact on the water mass distributions in the Yellow Sea. *Ocean Science Journal*, *53*, 165–178. https://doi.org/10.1007/s12601-018-0013-3

Lorenc, A. C., & Rawlins, F. (2005). Why does 4D-Var beat 3D-Var? *Quarterly Journal of the Royal Meteorological Society*, *131*, 3247–3257. https://doi.org/10.1256/qj.05.85

Lorenz, E. N. (1963). Deterministic nonperiodic flow. *Journal of Atmospheric Sciences*, *20*(2), 130–141. https://doi.org/10.1175/1520-0469(1963)020<0130:dnf>2.0.co;2

Madec, G. (2008). *NEMO ocean engine*. Institut Pierre-Simon Laplace. Retrieved from http://www.nemo-ocean.eu//About-NEMO/Reference-manuals

Madec, G., & the NEMO Team. (2012). *Nemo Ocean Engine v3.4. Note du Pole de Modélisation*. Institut Pierre Simon Laplace. Retrieved from http://www.nemo-ocean.eu/27

McCarthy, G. D., Smeed, D. A., Johns, W. E., Frajka-Williams, E., Moat, B. I., Rayner, D., et al. (2015). Measuring the Atlantic meridional overturning circulation at 26°N. *Progress in Oceanography*, *130*, 91–111. https://doi.org/10.1016/j.pocean.2014.10.006

Meinen, C. S., Baringer, M. O., & Garcia, R. F. (2010). Florida Current transport variability: An analysis of annual and longer-period signals. *Deep Sea Research Part I: Oceanographic Research Papers*, *57*(7), 835–846. https://doi.org/10.1016/j.dsr.2010.04.001

Menard, R., & Daley, R. (1996). The application of Kalman smoother theory to the estimation of 4DVAR error statistics. *Tellus A*, *48*(2), 221–237. https://doi.org/10.1034/j.1600-0870.1996.t01-1-00003.x

Mirouze, I., Blockley, E. W., Lea, D. J., Martin, M. J., & Bell, M. J. (2016). A multiple length scale correlation operator with application to ocean data assimilation. *Tellus A*, *68*, 29744. https://doi.org/10.3402/tellusa.v68.29744

Miyoshi, T., Sato, Y., & Kadowaki, T. (2010). Ensemble Kalman filter and 4D-Var intercomparison with the Japanese operational global analysis and prediction system. *Monthly Weather Review*, *138*(7), 2846–2866. https://doi.org/10.1175/2010mwr3209.1

Mogensen, K., Balmaseda, M. A., & Weaver, A. (2012). *The NEMOVAR ocean data assimilation system as implemented in the ECMWF ocean analysis for System 4*.

Powell, B. S., Arango, H. G., Moore, A. M., Di Lorenzo, E., Milliff, R. F., & Foley, D. (2008). 4DVAR data assimilation in the intra-Americas sea with the Regional Ocean Modeling System (ROMS). *Ocean Modelling*, *23*(3–4), 130–145. https://doi.org/10.1016/j.ocemod.2008.04.008

Rio, M.-H., Mulet, S., & Picot, N. (2014). Beyond GOCE for the ocean circulation estimate: Synergetic use of altimetry, gravimetry, and in situ data provides new insight into geostrophic and Ekman currents. *Geophysical Research Letters*, *41*(24), 8918–8925. https://doi.org/10.1002/2014GL061773

Roberts-Jones, J., Bovis, K., Martin, M. J., & McLaren, A. (2016). Estimating background error covariance parameters and assessing their impact in the OSTIA system. *Remote Sensing of Environment*, *176*, 117–138. https://doi.org/10.1016/j.rse.2015.12.006

Ryan, A. G., Regnier, C., Divakaran, P., Spindler, T., Mehra, A., Smith, G. C., et al. (2015). GODAE OceanView Class 4 forecast verification framework: Global ocean inter-comparison. *Journal of Operational Oceanography*, *8*(1), s98–s111. https://doi.org/10.1080/1755876X.2015.1022330

Smith, D. M., Cusack, S., Colman, A. W., Folland, C. K., Harris, G. R., & Murphy, J. M. (2007). Improved surface temperature prediction for the coming decade from a global climate model. *Science*, *317*, 796–799. https://doi.org/10.1126/science.1139540

Smith, P. J., Fowler, A. M., & Lawless, A. S. (2015). Exploring strategies for coupled 4D-Var data assimilation using an idealised atmosphere–ocean model. *Tellus A: Dynamic Meteorology and Oceanography*, *67*(1), 27025. https://doi.org/10.3402/tellusa.v67.27025

Storkey, D., Blaker, A. T., Mathiot, P., Megann, A., Aksenov, Y., Blockley, E. W., et al. (2018). UK Global Ocean GO6 and GO7: A traceable hierarchy of model resolutions. *Geoscientific Model Development*, *11*, 3187–3213. https://doi.org/10.5194/gmd-11-3187-2018

Tanimoto, Y., Hanawa, K., Toba, Y., & Iwasaka, N. (1993). Characteristic variations of sea surface temperature with multiple time scales in the North Pacific. *Journal of Climate*, *6*(6), 1153–1160. https://doi.org/10.1175/1520-0442(1993)006<1153:cvosst>2.0.co;2

Troccoli, A., & Haines, K. (1999). Use of the temperature–salinity relation in a data assimilation context. *Journal of Atmospheric and Oceanic Technology*, *16*(12), 2011–2025. https://doi.org/10.1175/1520-0426(1999)016<2011:uottsr>2.0.co;2

Uotila, P., Goosse, H., Haines, K., Chevallier, M., Barthélemy, A., Bricaud, C., et al. (2018). An assessment of ten ocean reanalyses in the polar regions. *Climate Dynamics*, *52*(3), 1613–1650. https://doi.org/10.1007/s00382-018-4242-z

von Schuckmann, K., Le Traon, P. Y., Smith, N., Pascual, A., Brasseur, P., Fennel, K., et al. (2018). Copernicus marine service ocean state report. *Journal of Operational Oceanography*, *11*(1), S1–S142. https://doi.org/10.1080/1755876x.2018.1489208

Waters, J., Lea, D. J., Martin, M. J., Mirouze, I., Weaver, A., & While, J. (2015). Implementing a variational data assimilation system in an operational 1/4 degree global ocean model. *Quarterly Journal of the Royal Meteorological Society*, *141*, 333–349. https://doi.org/10.1002/qj.2388

Weaver, A. T., Deltel, C., Machu, E., Ricci, S., & Daget, N. (2005). A multivariate balance operator for variational ocean data assimilation. *Quarterly Journal of the Royal Meteorological Society*, *131*, 3605–3625. https://doi.org/10.1256/qj.05.119

Wunsch, C., Heimbach, P., Ponte, R. M., Fukumori, I., & ECCO-GODAE CONSORTIUM MEMBERS. (2009). The global general circulation of the ocean estimated by the ECCO-Consortium. *Oceanography*, *22*(2), 88–103. https://doi.org/10.5670/oceanog.2009.41

Zhu, J., Huang, B., & Balmaseda, M. A. (2012). An ensemble estimation of the variability of upper-ocean heat content over the tropical Atlantic Ocean with multi-ocean reanalysis products. *Climate Dynamics*, *39*(3–4), 1001–1020. https://doi.org/10.1007/s00382-011-1189-8